Non-linear optical properties of β-D-fructopyranose calcium chloride MOFs: an experimental and theoretical approach

Synthesis, structure and NLO properties of a new isostructural β-D-fructopyranose alkaline halides MOFs. A theoretical and experimental study.

Domenica Marabello*,[a,b] Paola Antoniotti,[a] Paola Benzi,[a,b] Carlo Canepa,[a] Leonardo Mortati,[d] Maria Paola Sassi[d]

[a]*Dipartimento di Chimica, Università degli Studi di Torino, Torino*

[b]*CrisDi-Interdepartmental Center for Crystallography, University of Torino*

[d]*INRIM – Istituto Nazionale di Ricerca Metrologica, Torino, Italy*

Abstract

In this work we investigated four isomorphous Metal Organic Frameworks, based on fructose and alkali-earth alogenides to better understand the effect of the size of the cation and the different polarizability of the anion on the calculated hyperpolarizability and optical susceptibility, that are correlated to NLO properties. The compounds were characterized by X-ray diffraction and the first hyperpolarizability and the second-order susceptibility were obtained from theoretical calculations. Furthermore, a new method to measure the SH efficiency on a small quantity of powder at different wavelengths of excitation was optimized and we attempted to assess the reduction of the SH intensity for small quantities of nano-crystals, in order to ascertain the possibility of applications in biological systems.

The results of this work show that both the intrinsic nature of the anion and the induced dissociation of cation and anion by fructose play a role for the SHG properties of such compounds.

Keywords: Metal Organic Frameworks, isomorphs materials, NLO properties, SHG efficiency, structure-properties relationship

Introduction

Non linear optical (NLO) materials are required for multiple applications in the fields of laser technology, optical communication and data storage technology (Agullo-Lopez *et al.*, 1995). Moreover, second-harmonic generating (SHG) materials can be used in biology and medicine for microscopic *in vivo* imaging technique (Pantazis *et al*., 2010, Dempsey *et al*., 2012, McKinlay *et al*., 2010). Inorganic materials are widely used in these applications, but the optical linearity of these is not satisfying in terms of SHG efficiency with respect to organic compounds, that can exhibit SHG efficiencies thousand times that of inorganic NLO materials (Tam *et al*., 1989). However, the organic NLO crystals are often difficult to growth, too fragile and also sometimes too chemically unstable for applications. In the past decades, some semi-organic materials combining the NLO properties of organic molecules with the stability of inorganic salts, were considered for NLO applications. For example, among metal-organic coordination compounds several complexes of aminoacids with inorganic salts have been surveyed (Jiang *et al*., 1999, Kupplera *et al*., 2009, Chandrasekaran *et al*., 2012, Dhanuskodi *et al*., 2007). In particular, Jiang *et al.* showed that a combination of inorganic and organic materials provides a potentially useful approach to more efficient and more stable NLO crystals, providing the advantages of both an enhancement of the physico-chemical stability and an increase in NLO intensity via the metal-ligand bridging interactions. In fact, both the central metal ion and the halogen anions are proved to be involved in the promotion of the SHG efficiency.

NLO materials require the lack of the inversion centre in the crystal structure; to fulfill this requirement in semi-organic materials, chiral organic ligands must be utilized, since pure inorganic salts more easily crystallize in centrosymmetric space groups. The presence of the asymmetric ligand drives the crystallization toward a new *non*-centrosymmetric material, and makes it a good candidate for the NLO properties. One difficulty in the synthesis of chiral organic ligands is the separation of the two enantiomers. For this reason in this work we considered carbohydrates ligands, naturally synthetized in only one enantiomer and also good asymmetric poly-dentate ligands that are able to coordinate alkaly-earth metals with formation of metal organic frameworks (MOFs). The SHG efficiency of many mono-, di- and tri-saccharides have been examined, and a correlation between their crystal systems and SHG efficiencies was evidenced, *i.e.* the lower is the space group symmetry of the crystal the larger its SHG efficiency (Bournill *et al*., 1993). In this work, we focused our attention on complexes of saccharide and inorganic salts also because of their non-toxic and bio-compatible properties, required for biological applications. Among inorganic salts, calcium and strontium compounds were considered, since these two metals are involved a variety of biological processes playing important physiological roles (e.g. calcium storage, bone calcification, and calcium-dependent interaction in cells) and consequently showing large biocompatibility (Kannan *et al*., 2010). Fructose was chosen as a carbohydrate ligand because of its large affinity toward alkaline-earth metals, its commercially availability and low cost.

In our previous work (Marabello *et al*., 2015), we reported a theoretical and experimental study on the NLO properties of two MOFs obtained from fructose and calcium chloride, $[Ca(C_6H_{12}O_6)_2(H_2O)_2]Cl_2{\cdot}H_2O$ (**CaFruCl**) and $[Ca(C_6H_{12}O_6)(H_2O)_2]Cl_2$ (**CaFruCl-2**). We measured (Mortati *et al*., 2012) their SH intensity by SHG microscopy and we showed that the coordination of fructose on the calcium ion improves the SH efficiency with respect to fructose itself, probably by both the induced lowering of symmetry and the dissociation of $CaCl_2$. In this work we extended our investigation on MOFs obtained from fructose and other alkali-earth alogenides to better understand the effect of the size of the cation and the different polarizability of the anion in isomorphous structures on the calculated hyperpolarizability and optical susceptibility, which in turn are related to the SHG efficiency. In particular, we synthetized more isomorphs of **CaFruCl** of formula $[M(C_6H_{12}O_6)_2(H_2O)_2]X_2{\cdot}H_2O$, with M=Ca, Sr and X=Cl, Br. Few

complexes of fructose and inorganic salts are known in the literature (Craig et al., 1974, Cook & Bugg, 1975, Guo & Zhang, 2004), and for all of them the synthesis methodology implies the very slow evaporation of acqueous solutions with procedures that completed in several months. In this work, we instead optimized a new simple, rapid and low-cost synthesis methodology, free of any environmental impact. The compounds were characterized by X-ray diffraction and the resulting coordinates of the crystal fragments were used both to optimize, at the B3LYP level of theory, the geometries of the complexes and to calculate first hyperpolarizability (β) and second-order susceptibility ($\chi^{(2)}$). Since these compounds share the same crystalline structure, they represent an interesting opportunity to investigate how the SHG properties change with the nature of the cation and the anion. Furthermore, since most biological applycations of NLO materials in recent years involve powdered samples (Haber *et al*., 2011, Wunderlich *et al*., 2013, Bäumner *et al*., 2010, Staedler *et al*., 2012), we to optimized a new method to measure the SHG efficiency on a small quantity of powder at different wavelengths of excitation, trying to determine the quadratic coefficient relevant to the second-order susceptibility. Furthermore, we also attempted to assess reduction of the SH intensity for small quantities of nano-crystals, in order to ascertain the possibility of applications in biological systems.

Experimental

Synthesis of $[Ca(C_6H_{12}O_6)_2(H_2O)_2]Cl_2{\cdot}H_2O$ (**CaFruCl**). The synthesis and X-ray structure determination of this compound is reported in our previous work (Marabello *et. al*, 2015).

Synthesis of $[Ca(C_6H_{12}O_6)_2(H_2O)_2]Br_2{\cdot}H_2O$ (**CaFruBr**). Calcium bromide and β-D-fructose were ground together into an agate morthar at the stoichiometric ratio 1:2 and subsequently partially dissolved in a small amount of ethanol at room temperature. The solution at equilibrium with its solid was closed into a vial and numerous crystals of the compound were deposited on the walls of the vial after few days. These crystals were filtered on paper and quickly dried under air flux at room temperature. The X-ray crystal structure of this compound was determined by Cook & Bugg on 1976 but, since the X-ray characterization was very old the X-ray structure of this compound was re-determined in order to obtain more accurate data for the comparison with the compounds investigated in this work.

Synthesis of $[Sr(C_6H_{12}O_6)_2(H_2O)_2]Cl_2{\cdot}H_2O$ (**SrFruCl**). Anhydrous calcium chloride and β-D-fructose were dissolved in ethanol at 348 K in the stoichiometric ratio 1:2. During the dissolution of the reagents a faint precipitate is deposited at the bottom of the solution. The solution was filtered and slowly evaporated at room temperature in a glass test-tube. After few days a crystalline powder was deposited on the wall of the test-tube. These crystals were filtered on paper and quickly dried under air flux at room temperature. The X-ray crystal structure of this compound was determined by Guo & Zhang on 2004 and for this work data deposited on the CSD data bank were utilized (CCDC 220667).

Synthesis of $[Sr(C_6H_{12}O_6)_2(H_2O)_2]Br_2{\cdot}H_2O$ (**SrFruBr**). Calcium bromide and β-D-fructose were completely dissolved in ethanol at 348 K in the stoichiometric ratio 1:2. The solution was slowly evaporated at room temperature in a glass test-tube and after few days a crystalline powder was deposited on the wall of the test-tube. These crystals were filtered on paper and quickly dried under air flux at room temperature.

X-ray diffraction. X-ray diffraction data for compounds **CaFruBr** and **SrFruBr** were collected at room temperature using an Oxford Diffraction Gemini R Ultra diffractometer. Data were collected with graphite monocromatized Mo-Kα radiation (0.71073 Å). The CrysAlisPro [CrysAlisPro, 2014] package was used for data collection and integration, SHELXT (Sheldrick, 2015) for resolution, SHELXL (Sheldrick, 2015) for refinement and Olex2 [Dolomanov *et al.*, 2009] for graphics.

Both compounds crystallize in the monoclinic C2 space group with Z=2. All but the hydrogen atoms were anisotropically refined. All H atoms were located on difference Fourier maps, but they were calculated and refined riding with U_{iso}=1.2 or 1.5 U_{eq} of the bonded atom. Compound **3**: 7940 reflections measured, 3298 unique (R_{int} = 0.0364), R1(F^2)= 0.0335, *w*R(F^2)= 0.0716, max/min peak = 0.35/-0.56, CCDC 1511464. Compound **5**: 11419 reflections measured, 5390 unique (R_{int} = 0.0438), R1(F^2)= 0.0497, *w*R(F^2)= 0.0805, max/min peak = 0.51/-0.89, CCDC 1511467.

Details of crystal data for all compounds are reported in Table 1.

Computational methods. The calculations were performed with the GAUSSIAN09 set of programs (Gaussian 09, 2009). All the structures in this work were optimized by gradient-based techniques (Schlegel & Daudel, 1981, Schlegel, 1982, Schlegel *et al.*, 1984) without symmetry constraints at the DFT B3LYP (Becke, 1988, Becke, 1993) level of theory, in conjunction with the 6-31G(d) basis set (Hehre *et al.*, 1986). All critical points were characterized as energy minima, by analytical calculation of vibrational frequencies. Total dipole moments, polarizabilities and first order hyperpolarizabilities were calculated at the same level of theory. Molecular volumes were computed by averaging ten different volume calculations on the optimized geometries at the B3LYP/6-31G(d) level of theory with the Gaussian09 options scf=tight, volume=tight, and iop(6/45=500,6/46=1) (Parsons, & Ninham, 2009).

Second Harmonic Generation Spectral Measurements. All compounds were characterized in terms of second harmonic generation emission, using a NLO Multimodal microscope described earlier [Mortati *et al*., 2012]. The powdered compounds, with each individual crystal in random orientation, were analyzed acquiring averaged images at different excitation wavelengths and powers, keeping the detector setting parameters (i.e. PMT voltage, gain and offset) fixed for all the measurements.

The measurements were repeated and averaged five times. Each image was processed by computing the average intensity related to the actual sample surface obtained by masking the image through an Otsu's threshold binary mask, avoiding the background contribution. The computed averages were quadratically fitted with the actual sample excitation powers excluding all the outliers to improve the curve fitting, using a method described in a previous work (Marabello *et al*., 2015). In this work, the quadratic coefficients were extracted for different excitation wavelengths in a spectral range between 900 and 940 nm and they were grouped per wavelengths with a binning size of about 6 nm. The resulted mean values are plotted together with error bars related to the standard deviation of the averages in the selected bin (Fig. 3). The wavelength range was chosen according to the filter setup range in order to reject excitation source and measure the actual SH signal.

Results and discussion

X-ray structures. Compounds **CaFruCl, CaFruBr, SrFruCl** and **SrFruBr** are isomorphs, that is atoms show the same disposition in the cell, crystallizing in the same space group. The cell volumes are only slightly different so that these compounds can be effectively considered as isomorphs (Table 1).

Table 1

The asymmetric unit of all compounds contains one fructose molecule, one half of a calcium ion, one chloride, one water molecule coordinated to the calcium ion and one half of a free water molecule. Analyzing the crystal packing, two

fructose molecules bridge two metal ions, and an infinite thread of fructose and calcium ions develops in the [010] direction (Figure 1). Consequently, these compounds have to be thought of as uni-dimensional Metal Organic Framework (1D-MOF) of a special type, since the multi-dentate ligand is a neutral molecule (fructose), while the metal atom is +2 charged. The halogen ions and the free water molecules are inserted between the Ca-fructose threads, strictly connected through strong hydrogen bonds to the sugar molecules and to the water molecules coordinated to the metal. Those bonds contribute to stabilize the crystal. The hydrogen bond distances and angles for all compounds are listed in the supporting informations.

Figure 1

As can be observed from the data in table 1, the main difference in structure among the four compounds is the cell volume, in turn influenced by the different volumes of the ions involved. Comparing the pairs **CaFruCl**/**SrFruCl** and **CaFruBr**/**SrFruBr** (different alkaline-earth metal, but same halogen anion for each pair) the expected increase in cell volume induced by the heavier atom (from Ca to Sr), is lower with respect to corresponding increase of the pairs **CaFruCl**/**CaFruBr** and **SrFruCl**/**SrFruBr** (same metal, different halogen anion). Thus, the presence of bromide atom implies a significant increase of cell volume with respect to the chloride, while the change from Ca to Sr exerts a smaller influence on the enlargement of the structure. In figure 2 the environment around the metal atom is shown and in Table 2 the relevant distances are reported.

Figure 2

Table 2

Comparing the averaged values of the distances M^{2+}-O_{FRU}, M^{2+}-O_W, $M^{2+}\cdots M^{2+}$ and $M^{2+}\cdots X^-$, different trends are observed. While M^{2+}-O_{FRU} and M^{2+}-O_W bonds are significantly influenced by the cation, the $M^{2+}\cdots M^{2+}$ distances increase gradually from **CaFruCl** to **SrFruBr** and this reflects in the elongation of the b-axis (see table 1). On the contrary, the $M^{2+}\cdots X^-$ distances are influences mainly by the anion, mirroring the behavior of the cell volumes. In practice, we observe a gradual elongation of the metal-sugars "thread" from **CaFruCl** to **SrFruBr**, but the transversal connections with the anions show constant distances in the pairs **CaFruCl**/**SrFruCl** and **CaFruBr**/**SrFruBr**.

Computational results. The geometries of the four complexes were obtained by optimizing the atomic coordinates from the X-ray experiments of the crystal fragments shown in Figure 1, composed of three calcium ions, six fructose molecules, nine water molecules and six chloride ions. In Table 2 the optimized atomic distances of the complexes are compared to the corresponding values from X-ray diffraction. The reported values are in good agreement, showing small deviations, probably due to the intermolecular interactions in the crystalline state. The maximum difference between the average bond lengths M^{2+}-O_{FRU} in the four compounds, is observed for SrFruBr and it does not exceed 0.075 Å. The larger deviation for the M^{2+}-O_W average bonds is not higher than 0.15 Å. Regarding the average distances $M^{2+}\cdots X^-$, the larger deviation is observed in CaFruBr, between Ca^{2+} and Br^- and is 0.55 Å. However, the increase in distance from $M^{2+}\cdots Cl^-$ to $M^{2+}\cdots Br^-$, observed from X-ray diffraction, is well reproduced both for the calcium compounds and for the strontium ones.

In Table 3 the computed values of dipole moment (μ), mean polarizability ($<\alpha>$), first static hyperpolarizability (β_{tot}) and second-order susceptibility ($\chi^{(2)}$) are reported for all compounds. These computed quantities, when obtained with a consistent level of theory and basis set, may be safely compared even in absence of experimental data.

The total dipole moments and the mean polarizabilities in a Cartesian frame are defined as (Kanis *et al*., 1994, Kyrill *et al.*, 2008)

$$\mu = \left(\mu_x^2 + \mu_y^2 + \mu_z^2\right)^{1/2} \quad (3)$$

$$< \alpha >= (1/3)\left(\alpha_{xx} + \alpha_{yy} + \alpha_{zz}\right). \quad (4)$$

The total intrinsic hyperpolarizability β_{tot} is defined as

$$\beta_{tot} = \left(\beta_x^2 + \beta_y^2 + \beta_z^2\right)^{1/2}. \quad (5)$$

where $\beta_x = \beta_{xxx} + \beta_{xyy} + \beta_{xzz}$, $\beta_y = \beta_{yyy} + \beta_{yzz} + \beta_{yxx}$, and $\beta_z = \beta_{zzz} + \beta_{zxx} + \beta_{zyy}$.

The relationship between the macroscopic second-order susceptibility and the microscopic total hyperpolarizability is given by Eq. (6).

$$\chi^{(2)} = NF\beta_{tot} \ , \quad (6)$$

where N is the number of particles *per* unit volume and F is the local field factor, assumed to be one. Since F depends on crystal symmetry, and the compounds studied in this work have the same structure, for all compounds the same value was attributed to F.

Table 3 shows that the values of the total dipole moment, polarizability and hyper-polarizability for these compounds are similar, with some systematic differences due to the composition of the compounds. The dipole moment is more affected by the cation, the compounds with calcium having a dipole moment greater than those with strontium. Instead, the polarizability and hyper-polarizability values are more influenced by the anion, the compounds that contain the bromine anion showing the highest values.

The calculated static susceptibility $\chi^{(2)}$ values for the compounds with bromine anion are larger than the corresponding compound with chloride anion (the difference in $\chi^{(2)}$ is 0.6 pm/V from **CaFruCl** to **CaFruBr** and 0.42 pm/V from **SrFruCl** to **SrFruBr**). On the other hand, a comparison of the values between compounds containing the same anion but different cations shows different cations only slightly influence the $\chi^{(2)}$ values.

Thus, being the hyperpolarizability and static susceptibility values correlated to the SHG properties of the compounds, theoretical calculations of these quantities suggest that compounds with the greatest and more polarizable anion should show higher SHG properties, while the cation does not play a significant role in determining the SHG property.

Second Harmonic Generation Analysis

In Figure 3 the extracted quadratic fitting parameters of the SH intensities in function of the excitation power at different excitation wavelengths for all the analyzed compounds are plotted.

Figure 3

Taking into account the variability of the measurements, Figure 3 shows that the compounds considered in this work do not show large differences in SH intensity at all the excitation wavelengths considered. This behavior suggests that the SHG efficiency mainly depends on their structural assembly, which is the same for all compounds. Furthermore, for the compounds containing the calcium ion the SH intensity seems on average higher at almost all the excitation wavelengths with respect to the compounds containing strontium. In particular, compound **2** has two peaks when excited with wavelengths around 920 and 935 nm. From the chemical point of view, the measured SH intensity agrees with the calculated values of β_{tot} and $\chi^{(2)}$ that suggest similar NLO behavior for all these compounds. On the other end, while the computed increase of SH intensity in the presence of Br^- instead of Cl^- is confirmed by experiments for the Sr compounds (**SrFruBr** with respect to **SrFruCl**), for the Ca compounds (**CaFruCl** and **SrFruBr**) this behavior is

unclear. The experimental values refer to a global behavior of powders and can be affected by several sources of uncertainty. Consequently, caution must be exercised in comparing these compounds. Uncertainties involve optical aspects, like local transmittance of the optical signals towards the sample or the detector, and the scattering of the emitted light through the powder itself. The using of microscope objectives ensures a limitation on the depth of field of the order of a few micrometers, even if the local thickness of the powder is not constant in all the samples. The objective focal volume reasonably confines the SH emitted intensity, due to the nonlinear optical nature of the SH process that requires a high local concentration of photons to be generated with higher probability. The variation of the powder thickness, however, could affect the transmittance of the samples and thus partially affects the comparability of the results. Due to the hygroscopic nature of some of the samples, it was not possible to obtain constant thickness of all the samples. This fact could partially account for the differences between experimental and theoretical data in this work. Since the compounds studied in this work exhibit some features that could be interesting for biomedicine applications, one would want to estimate the observed intensity in the operating conditions for SH microscopy. To this purpose, assumptions have to be made, namely the absence of phase match and the smallness of crystal size with respect to the coherence length. The SH intensities were measured sampling layers with thickness $30 < h < 100$ μm. The stack of particles inside a biological cell, each of size 0.5 μm, would reasonably have thickness $h' = 2$ μm and, based on the model of Perry (Kurtz & Perry,1968), one would expect the intensity to be lowered by a factor $0.02 < h'/h < 0.07$. We anticipate the resulting SH intensity to be detectable by an NLO multimodal microscope.

Conclusions

In this work, we had the unusual possibility to analyze four fructose-salt compounds sharing the same structure with different combinations of Ca/Sr and Cl/Br ions. Theoretical calculations suggested that the SH efficiency is much influenced by the anion, the first static hyperpolarizability and second order susceptibility being higher for bromide compounds with respect to those with chloride. On the contrary, the cation seems not to play a significant role in the SHG properties. The structure analysis evidenced that the compounds containing bromide show a significant difference in the cell volumes with respect to the compounds with chlorine, mainly due to longer cation-anion distances. These results confirms that both the intrinsic nature of the anion and the induced dissociation of M···X by fructose play a role for the SHG properties of such compounds, as suggested in our previous work [Marabello *et al.*, 2015].

Experimental SHG measurements of SH intensity on these compounds have similar values, considering experimental errors. This similarity was expected since they share the same structure. However, the relative SH intensities remain unexplained, due to both uncertainty in measurements and the difficulties caused by the hygroscopic behavior of these compounds. Finally, we estimated the SH intensity in operative biological environment and one would expect that these compounds should be suitable for biological applications.

References

Agullo-Lopez, F., Cabrera, J.M. & Agullo-Rueda, F. (1994). *Electrooptics: Phenomena, Materials and Applications*. New York: Academic Press.

Bäumner, R., Bonacina, L., Enderlein, J., Extermann, J., Fricke-Begemann, T., Marowsky, G., & Wolf, J-P. (2010). *Opt. Express* **18**, 23218-23225

Becke, A.D. (1988). *Phys. Review* A**38**, 3098–3100

Becke, A.D. (1993). *J. Chem. Phys.* **98**, 5648

Bournill, G., Mansour, K., Perry, K. J., Khundkar, L., Sleva, E. T., Kern, R. & Perry, J. W. (1993). *Chem. Mater.* **5**, 802-808

Chandrasekaran, J., Ilayabarathi, P., Maadeswaran, P., Kutty, P. M. & Pari, S. (2012). *Optics Commun*. **285**, 2096-2100

Cook, W. J. & Bugg, C. E. (1975). Acta Cryst. B**32**, 656

Craig, D.C., Stephenson & N.C., Stevens, J.D. (1974). *Cryst. Struct. Commun*. **3**, 195

Craig, D.C., Stephenson & N.C., Stevens, J.D. (1974). *Cryst. Struct. Commun*. **3**, 277

CrysAlisPro, Agilent Technologies, Version 1.171.37.31 (release 14-01-2014 CrysAlis171 .NET, compiled Jan 14 2014,18:38:05)

Dempsey, W.P., Fraser, S.E. & Pantazis , P. (2012). *Bioessays* **34**, 351–360

Dhanuskodi, S., Vasantha, K. & Angely Mary, P. A. (2007). *Spectrochimica Acta, Part A* **66**, 637-642

Dolomanov, O.V., Bourhis, L.J., Gildea, R.J, Howard, J.A.K. & Puschmann, H. (2009). *J. Appl. Cryst*. **42**, 339-341

Gaussian 09, Revision A.02, Frisch, M. J., Trucks, G. W., Schlegel, H. B., Scuseria, G. E., Robb, M. A., Cheeseman, J. R., Scalmani, G., Barone, V., Mennucci, B., Petersson, G. A., Nakatsuji, H., Caricato, M., Hratchian, X., Li, H. P., Izmaylov, A. F, Bloino, J., Zheng, G., Sonnenberg, J. L., Hada, M., Ehara, M., Toyota, K., Fukuda, R., Hasegawa, J., Ishida, M., Nakajima, T., Honda, Y., Kitao, O., Nakai, H., Vreven, T., Montgomery, J. A., Peralta, Jr. J. E., Ogliaro, F., Bearpark, M., Heyd, J. J., Brothers, E., Kudin, K. N., Staroverov, V. N., Kobayashi, R., Normand, J., Raghavachari, K., Rendell, A., Burant, J. C., Iyengar, S. S., Tomasi, J., Cossi, M., Rega, N., Millam, J. M., Klene M., Knox, J. E., Cross, J. B., Bakken, V., Adamo, C., Jaramillo, J., Gomperts, R., Stratmann, R. E., Yazyev, O., Austin, A. J., Cammi, R., Pomelli, C., Ochterski, J. W., Martin, R. L., Morokuma, K., Zakrzewski, V. G., Voth, G. A., Salvador, P., Dannenberg, J. J., Dapprich, S., Daniels, A. D., Farkas, Ö., Foresman, J. B., Ortiz, J. V., Cioslowski, J. & Fox, D. J. (2009). Gaussian, Inc., Wallingford CT

Guo, J. & Zhang, X. (2004). *Carbohydr. Res.* **339**, 1421-1426

Haber, L. H., Kwok, S.J.J., Semeraro, M. & Eisenthal, K.B. (2011). *Chem. Phys. Lett*. **507**, 11–14

Hehre, W.J., Radom, L., Schleyer, P.vR. & Pople, J.A. (1986). *Ab initio Molecular Orbital Theory*. Wiley, New York,

Jiang, M. & Fang, Q. (1999). *Adv. Mat*. **11**, 1147-1151

Kanis, D. R., Ratner, M. A., Marks, T. J. (1994). *Chem. Rev.* **94**, 195-242

Kannan, S., Goetz-Neunhoeffer, F., Neubauer, J. & Pina, S., Torres P.M.C., Ferreira, J.M.F. (2010). *Acta Biomaterialia* **6**, 571-576

Kuppler, R. J., Timmons, D. J., Fang, Q.-R., Li, J.-R., Makal, T. A., Young, M. D., Yuan, D., Zhao, D., Zhuang W. & Zhou H.-C. (2009). *Coordination Chemistry Reviews* **253**, 3042–3066

Kurtz, S.K. & Perry, T.T. (1968), *J. Appl. Phys*. **39**, 3798-3813

Kyrill, Y., Suponitsky, K. Y., Tafur, S., Masunov, A. E. J. (2008). *Chem. Phys.* **129**, 044109.1-044109.11

Marabello, D., Antoniotti, P., Benzi, P., Canepa, C., Diana, E., Operti, L., Mortati, L. & Sassi, M. P. (2015). *J. Mater. Sci.*, **50**, 12, 4330- 4341

McKinlay, A.C., Morris, R.E., Horcajada, P., Férey, G., Gref, R., Couvreur, P. & Serre C. (2010). *Angew. Chem. Int. Ed.* **49**, 6260 – 6266.

Mortati, L., Divieto, C. & Sassi, M. P. (2012). *J. Raman Spectrosc,* **43**, 675–680

Pantazis, P., Maloney, J., Wu, D. & Fraser, S.E. (2010). *Proceedings of the National Academy of Sciences of the United States of America* **107,** 14535–14540.

Parsons, D. F. & Ninham, B. W. (2009). *J. Phys. Chem. A* **113**, 1141-1150.

Schlegel, H.B. & Daudel, C. (1981). *Computational Theoretical Organic Chemistry*, Reidel Publ, Co.

Schlegel, H.B. (1982). *J. Chem. Phys.* **77**, 3676-3681

Schlegel, H.B. (1982). *J. Comput. Chem*. **3**, 214-218

Schlegel, H.B., Binkley, J.S. & Pople, J.A. (1984). *J. Chem. Phys.* **80**, 1976-1981

Sheldrick, G.M. (2015). *Acta Cryst*. A**71**, 3-8

Sheldrick, G.M. (2015). *Acta Cryst*. C**71**, 3-8

Staedler, D., Magouroux, T., Hadji, R., Joulaud, C., Extermann, J., Schwung, S., Passemard, S., Kasparian, C., Clarke G., Gerrmann M., Le Dantec R., Mugnier Y., Rytz D., Ciepielewski D., Galez C., Gerber-Lemaire S., Juillerat-Jeanneret, L., Bonacina, L. & Wolf, J-P. (2012). *ACS Nano* **6**, 2542-2549

Tam, W., Guerin, B., Calabrese, J. C. & Stevenson, S. H. (1989). *Chem. Phys. Lett.* **154**, 93-96

Wunderlich, S. & Peschel, U. (2013). *Opt. Express* **21**, 18611-18623

Table 1. Cell parameters for compounds **CaFruCl**, **CaFruBr**, **SrFruCl** and **SrFruBr**.

Compound	**CaFruCl**	**CaFruBr**	**SrFruCl**	**SrFruBr**
Crystal system	Monoclinic			
Space group, Z	C2, 4			
a (Å)	16.016(1)	16.1449(7)	16.252(5)	16.439(1)
b (Å)	7.8393(2)	7.8881(3)	7.941(2)	8.0240(5)
c (Å)	10.8679(9)	11.4702(5)	10.751(3)	11.1931(8)
β (°)	127.82(1)	128.842(4)	127.652(4)	128.142(7)
V ($Å^3$)	1077.9(2)	1137.8(1)	1098.5(5)	1161.2(2)

Table 2. Relevant distances around the metal atom from X-ray data and B3LYP/6-31G(d) calculations. O_{FRU} = oxygen atoms of fructose molecules; O_W = oxygen atoms of water molecules coordinated to the metal ions.

	CaFruCl		**CaFruBr**		**SrFruCl**		**SrFruBr**	
	XRD	B3LYP	XRD	B3LYP	XRD	B3LYP	XRD	B3LYP
M(1)-O(2)	2.494(2)	2.486	2.486(3)	2.512	2.619(2)	2.662	2.618(4)	2.665
M(1)-O(2A)^{i}		2.501		2.536		2.643		2.651
M(1)-O(3)	2.462(2)	2.571	2.470(3)	2.509	2.591(3)	2.634	2.606(3)	2.642
M(1)-O(3A)^{i}		2.544		2.531		2.663		2.666
M(1)-O(6B)^{ii}	2.455(2)	2.567	2.468(3)	2.527	2.579(2)	2.712	2.614(3)	2.725
M(1)-O(6C)^{iii}	2.455(2)	2.520		2.511		2.702		2.779
M(1)-O(1W)	2.450(2)	2.622	2.450(3)	2.522	2.550(4)	2.665	2.557(4)	2.666
M(1)-O(1WA)^{i}		2.502		2.681		2.679		2.679
M(1)-X(1)	5.079(1)	4.200	5.258(1)	4.308	5.058	4.284	5.224(1)	4.471
M(1)-X(1A)^{i}		4.532		4.380		4.256		4.658
M(1)-X(1B)^{ii}	4.852(1)	4.655	5.051(1)	4.801	4.877	5.066	5.044(1)	4.872
M(1)-X(1C)^{iii}		4.744		4.946		4.899		4.820
M^{2+}-O_{FRU} av.	2.470	2.532	2.475	2.521	2.596	2.669	2.613	2.688
M^{2+}-O_W av.	2.450	2.562	2.450	2.602	2.550	2.672	2.558	2.672
$M^{2+}\cdots M^{2+}$	7.839	7.450	7.888	7.876	7.941	7.741	8.024	7.738
$M^{2+}\cdots X^{-}$ av.	4.966	4.533	5.155	4.609	4.968	4.626	5.134	4.705

Symmetry codes: (i) –x+2, y-1, -z-2 (ii) –x+2, y+1, -z+2; (iii) x, y-1, z

Table 3. Theoretically computed dipole moments μ (Debye), mean polarizabilities <α> (a.u.), first static hyperpolarizabilities β_{tot} (10^{-30} cm^5esu^{-1}), second order susceptibilities $\chi^{(2)}$ (pmV^{-1}).

	CaFruCl	**CaFruBr**	**SrFruCl**	**SrFruBr**
μ	44.108	42.678	38.793	38.204
<α>	691.078	741.549	680.171	728.274
β_{tot}	14.6	17.9	15.5	17.9
$\chi^{(2)}$	2.87	3.47	2.96	3.38

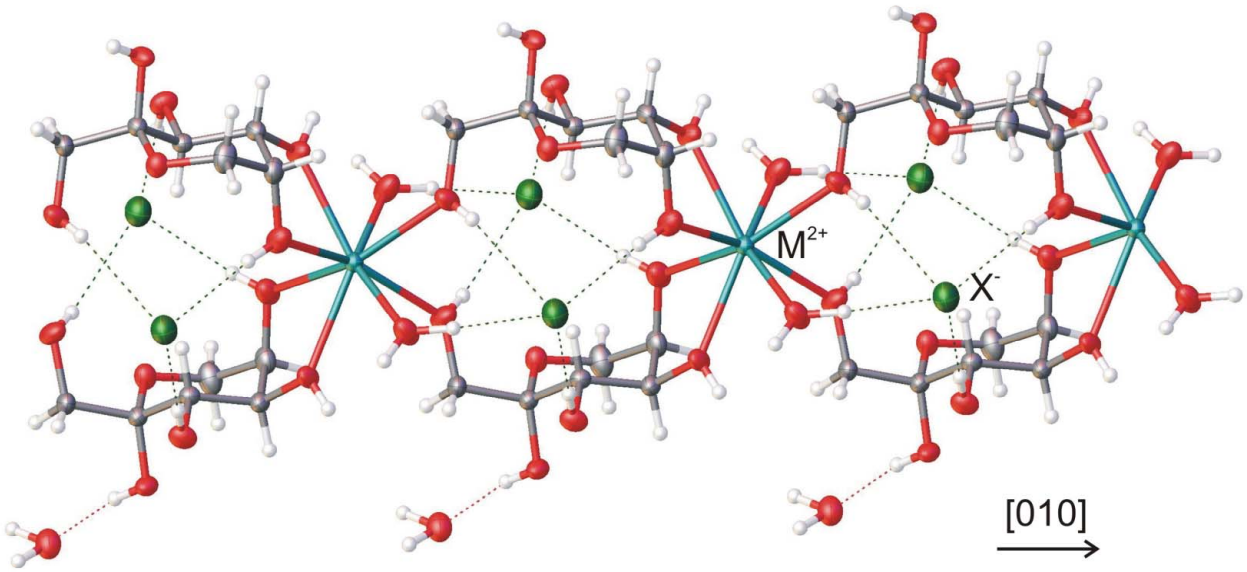

Figure 1. The infinite network of metal and halogen ions and sugar molecules for the structure of compounds **2**, **3**, **4,** and **5**.

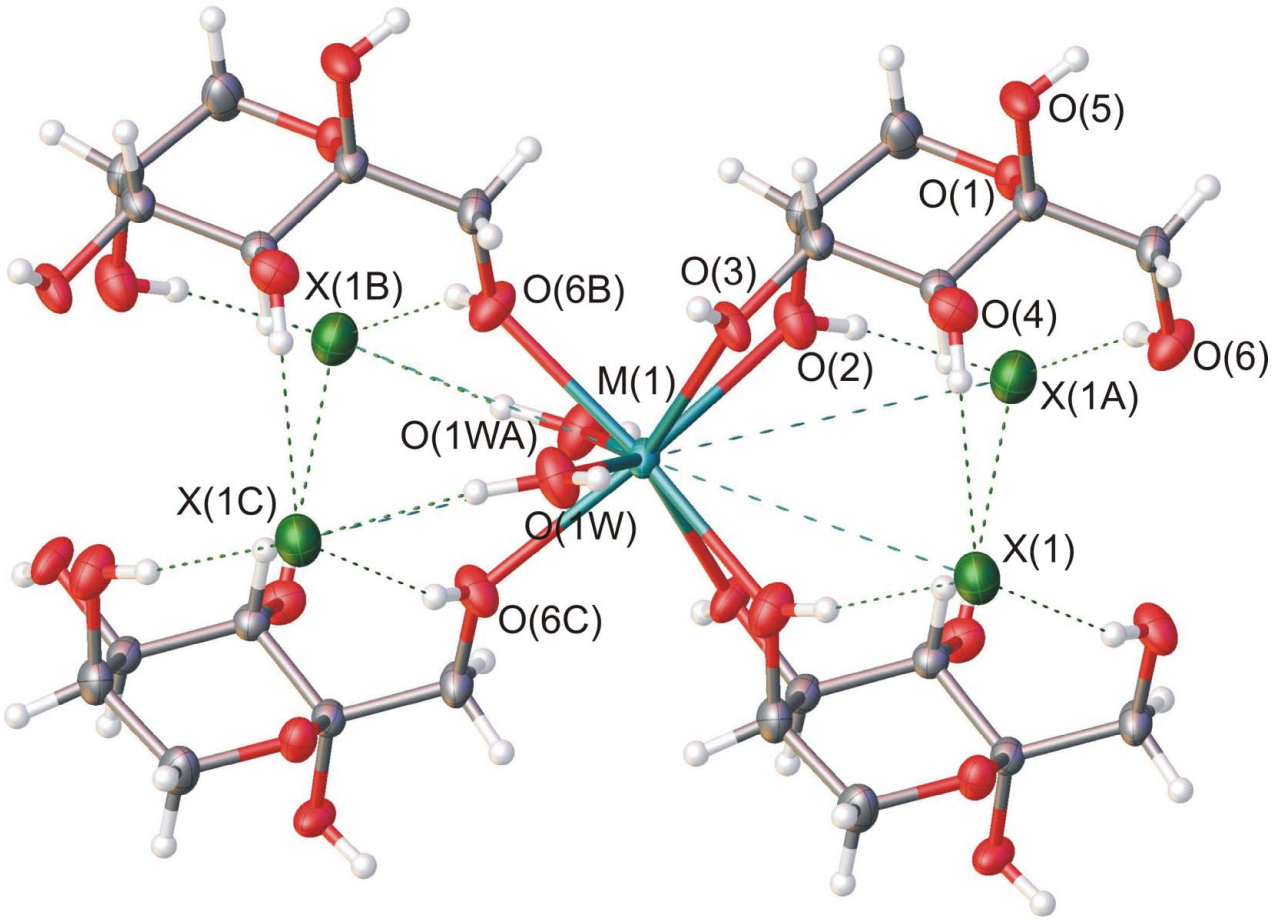

Figure 2. Coordination around the metal atom for compounds **2**, **3**, **4,** and **5**.

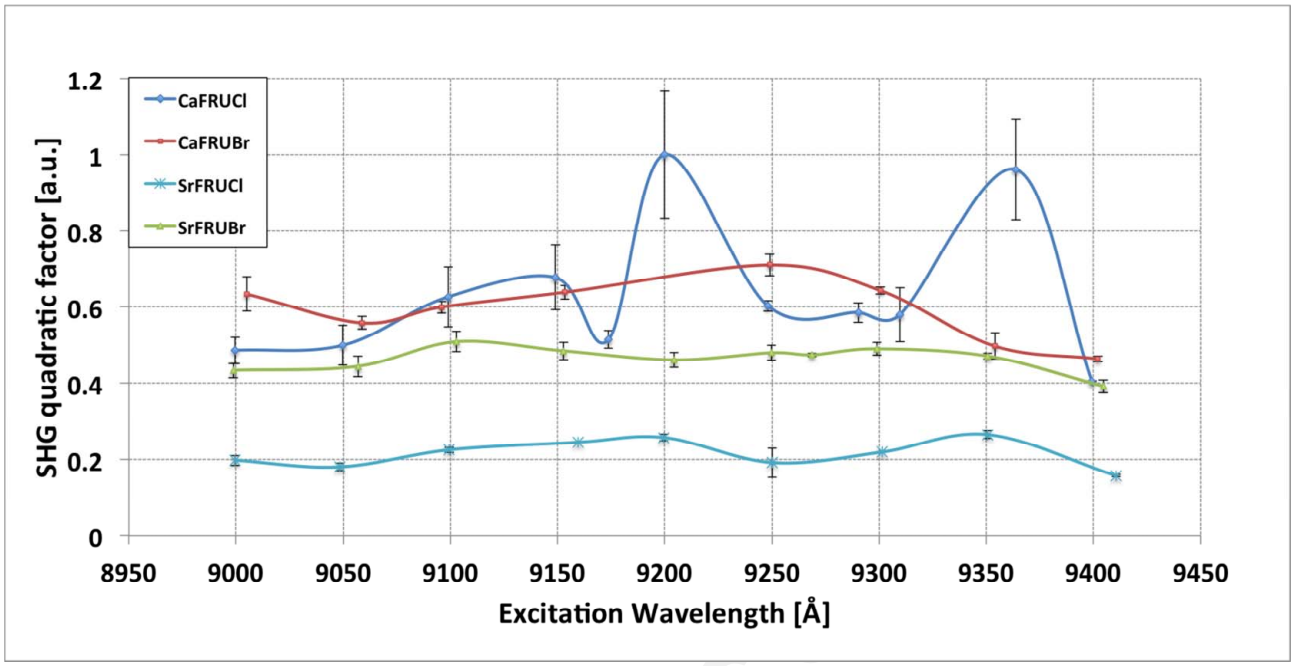

Figure 3. Quadratic fitting parameters (arbitrary units) of the SH intensities plotted in function of the excitation power at different excitation wavelengths for all the analyzed compounds. Error bars represent the standard deviations around the average point computed from the extracted quadratic fitting parameters.

Supporting informations

Table 1s. Hydrogen bond distances for compounds caFRUCl, CaFRUBr, SrFRUCl and SrFRUBr. X=Cl, Br.

D···A (Å) H···A (Å) D-H···A (°)	**CaFRUCl**	**CaFRUBr**	**SrFRUCl**	**SrFRUBr**
O4···X1^{i} H4···X1 O4-H4···X1		3.225(3) 2.41 170		
O5···O2W^{i} H5···O2W O5-H5···O2W		2.695(4) 1.88 172		
O6···O1^{i} H6···O1 O6-H6···O1		2.691(5) 2.26 113		
O1W···O5^{ii} H1WA···O5 O1W-H1WA···O5		2.880(6) 2.03 178		
O2···X1^{iii} H2···X1 O2-H2···X1		3.293(4) 2.45 173		
O1W···X1^{iv} H1WB···X1 O1W-H1W···X1		3.241 2.40 179		
O2W···X1^{v} H2W···X1 O2W-H2W···X1		3.193(3) 2.38 163		
O3···O4^{ii} H3···O4 O3-H3···O4		2.780(5) 2.00 152		
O6···X1^{iii} H6···X1 O6-H6···X1		3.673(4) 2.89 161		
C6···O4^{vi} H6B···O4 O6-H6···O4		3.314(6) 2.47 145		

i) 1555=x,y,z
ii) 4343=-x-1.5,y-0.5,-z-1.5
iii) 2353=-x-2,y,-z-2
iv) 1545= x, y-1, z
v) 3556=x+0.5,y+0.5,z+1.5
vi) 4353=-x-1.5, y+0.5, -z-1.5

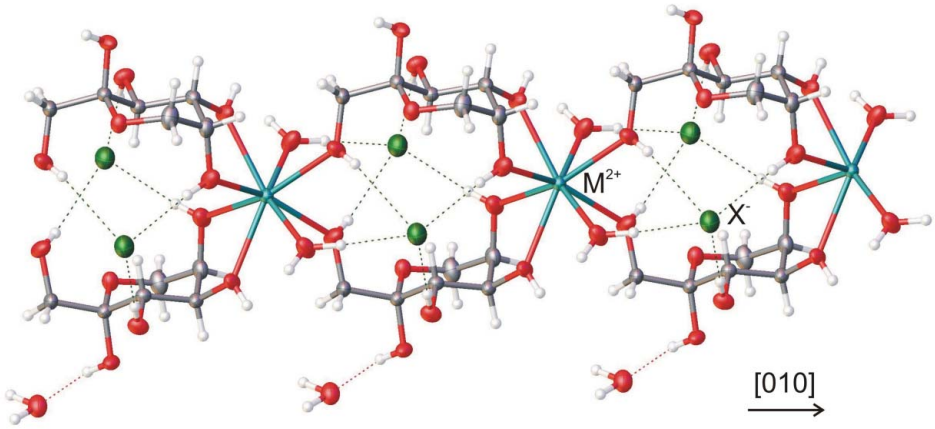

Figure 1

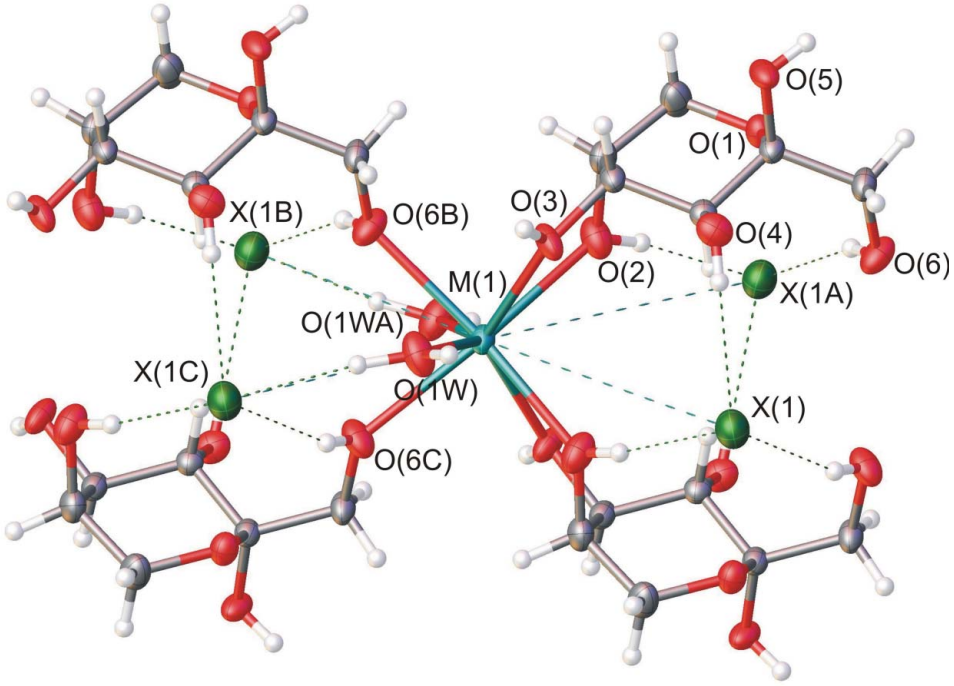

Figure 2

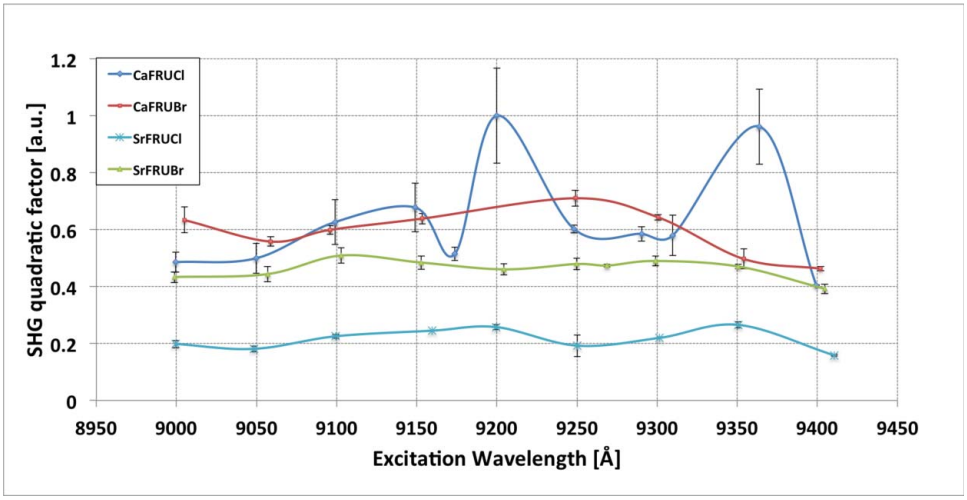
CaFRUCl
CaFRUBr
SrFRUCl
SrFRUBr
SHG quadratic factor [a.u.]
1.2
1
0.8
0.6
0.4
0.2
0
8950
9000
9050
9100
9150
9200
9250
9300
9350
9400
9450
Excitation Wavelength [Å]

Figure 3